

Dual Passivation of Perovskite and SnO₂ for High-Efficiency MAPbI₃ Perovskite Solar Cells

Yali Chen, Xuejiao Zuo, Yiyang He, Fang Qian, Shengnan Zuo, Yalan Zhang, Lei Liang, Zuqin Chen, Kui Zhao, Zhike Liu, Jing Gou,* and Shengzhong (Frank) Liu*

So far, most techniques for modifying perovskite solar cells (PSCs) focus on either the perovskite or electron transport layer (ETL). For the sake of comprehensively improving device performance, a dual-functional method of simultaneously passivating trap defects in both the perovskite and ETL films is proposed that utilizes guidable transfer of Eu³⁺ in SnO₂ to perovskite. Europium ions are distributed throughout the SnO₂ film during the formation process of SnO₂, and they can diffuse directionally through the SnO₂/perovskite interface into the perovskite, while most of the europium ions remain at the interface. Under the synergistic effect of distributed Eu³⁺ in the SnO₂ and aggregated Eu³⁺ at the interface, the electron mobilities of ETLs are evidently improved. Meanwhile, diffused Eu³⁺ ions passivate the perovskite to reduce trap densities at the grain boundaries, which can dramatically elevate the open-circuit voltage (V_{oc}) of PSCs. Finally, the mainly PSCs coated on SnO₂:Eu³⁺ ETL achieve a power conversion efficiency of 20.14%. Moreover, an unsealed device degrades by only 13% after exposure to ambient atmosphere for 84 days.

1. Introduction

The power conversion efficiency and device lifetime are both key factors for the assessing efficient perovskite solar cells. Recently, the certified power conversion efficiency (PCE) of perovskite solar cells (PSCs) has risen steeply to 23.7%,^[1–10] however, in comparison with commercial solar cells, such as crystalline silicon, polycrystalline silicon and Cu(In, Ga)Se₂ solar cells, the poor


device stability of PSCs is still the obstacle to obtaining a market share.^[11–13]

Most of the reported methods aiming to improve either or both the PCE and stability of PSCs focus on optimizing the perovskite or electron transport layer (ETL). Regarding perovskite photon absorber layers, their soft crystal lattices tend to easily deform, particularly under various stresses, such as moisture, oxygen, and ultraviolet light exposure, and even under the electric field and thermal stress during device operation.^[14–17] Various techniques, such as encapsulation, ultraviolet filtration, and modification have been used to delay the degradation of perovskite materials under the stress of environmental and device operational factors for maintaining long-term stability of PSCs. Additionally, methods that introduce additives into perovskite films to promote PCE are widely used.^[18,19] For instance, goethite quantum dots interact with iodine, lead and

methylamine, resulting in the retardation of crystallization kinetics to achieve perovskite films with high crystallinity and large grain size;^[20] Imidazole sulfonate zwitterions are introduced to regulate the crystal orientation of MAPbI₃ film so it is highly ordered to passivate trap states;^[21] and the conjugated polymer poly(bithiophene imide) is incorporated within grain boundaries to improve the crystallinity of perovskite film for reducing its defects.^[22]

Besides optimizing the photon absorber, as an important part of a PSC, the ETL must possess high electron mobility to extract photo-induced carriers because effectively transferring carriers to the external circuitry can promote the PCE of devices. Meanwhile, a suitable ETL should present decent optical transmittance for ensuring enough light reaches the perovskite absorber. Various strategies for optimizing ETLs are reported, such as ethylene diamine tetraacetic acid complexing SnO₂,^[23] using [6,6]-Phenyl C61 butyric acid to modify ZnO,^[24] or doping TiO₂ with Sm³⁺ and Eu³⁺ ions.^[25] Fabricating an ETL with organic chemicals or rare-earth ions can not only tune the Fermi level of the ETL to better match the conduction band of the perovskite for facilitating charge carrier transfer but also modify the interface between the perovskite and the ETL to induce the perovskite to crystallize with better quality and larger grain size. However, more effective and convenient techniques need to be developed to improve both the perovskite and ETL by simultaneously repairing the different trap defects in the photon absorber and ETL, finally achieving

Y. Chen, X. Zuo, Y. He, F. Qian, S. Zuo, Y. Zhang, L. Liang, Z. Chen, Prof. K. Zhao, Prof. Z. Liu, Prof. J. Gou, Prof. S. (Frank) Liu
Key Laboratory of Applied Surface and Colloid Chemistry
Ministry of Education
Shaanxi Key Laboratory for Advanced Energy Devices
Shaanxi Engineering Lab for Advanced Energy Technology
School of Materials Science and Engineering
Shaanxi Normal University
Xi'an 710119, China
E-mail: goujing@snnu.edu.cn; liusz@snnu.edu.cn

 The ORCID identification number(s) for the author(s) of this article can be found under <https://doi.org/10.1002/advs.202001466>

© 2021 The Authors. Published by Wiley-VCH GmbH. This is an open access article under the terms of the Creative Commons Attribution License, which permits use, distribution and reproduction in any medium, provided the original work is properly cited.

DOI: 10.1002/advs.202001466

effective photon-induced charge carrier separation and transfer for higher PCE. This one-step technique can reduce the cost of PSC engineering by a significant margin.

Europium ions can perform as a redox shuttle to selectively oxidize Pb^0 and reduce I^0 defects simultaneously in MAPbI_3 thin films, and the elimination of both Pb^0 and I^0 defects promotes the photovoltaic properties of MAPbI_3 PSCs with PCE up to 19.67%.^[10] This MAPbI_3 film is deposited by a traditional two-step method. In this process, $\text{Eu}(\text{acac})_3$ additive is added to the PbI_2/DMF (dimethylformamide) precursor solution. In addition to modifying the perovskite materials, Eu^{3+} and Sm^{3+} co-doped TiO_2 are prepared by the pulsed laser deposition method. The incorporated Eu^{3+} ions in cooperation with Sm^{3+} optimize the TiO_2 ETL, achieving higher electron extraction and lower interfacial recombination; therefore, power conversion efficiency as high as 19.01% can be obtained for a MAPbI_3 solar cell.^[25] Evidently, for the purpose of simultaneously reducing the trap defects in perovskite and ETL films, europium additive is a good choice; however, the above-discussed preparation methods present restrictive europium oxidation effects or high-temperature/cost synthesis processes.

We demonstrate a guidable transfer method to achieve Eu^{3+} incorporation in both the ETL and perovskite in one step. Europium and tin ions are simultaneously deposited to form $\text{SnO}_2:\text{Eu}^{3+}$ film on FTO (F-doped SnO_2) glass. We observed directional diffusion of Eu^{3+} from the SnO_2 ETL to the MAPbI_3 perovskite film, which leads to accumulation of large amount of Eu^{3+} at the perovskite/ETL interface. Eu^{3+} ions synergistically eliminate the trap defects in both the ETL and perovskite films, resulting in an improved electron mobility of the SnO_2 and grain boundary passivation within MAPbI_3 films. The champion fabricated PSC attains a PCE as high as 20.14%, and, when exposed to the ambient atmosphere, the unsealed PSC presents a slow degradation by only 13% after 84 days. All these results indicate that our dual-functional technique of europium passivation is extremely effective and convenient.

2. Results and Discussion

Since the refractive indices of FTO substrates and SnO_2 films are different, the reflectance can be influenced by the modification of SnO_2 films. Doping with Y^{3+} ions improves the antireflection ability of the SnO_2 films and results in an increase in the optical transmittance in the region of 350 to 625 nm for the substrates.^[26] The optical transmittance spectra of SnO_2 and $\text{SnO}_2:\text{Eu}^{3+}$ films on FTO substrates are shown in Figure 1a. It is interesting to note that doping Eu^{3+} ions can improve the optical transmission properties of FTO/ SnO_2 substrates. In both the 350–410 nm and 440–600 nm regions, the optical transmittances of FTO/ SnO_2 substrates are enhanced with increasing concentration of Eu^{3+} dopant.

The variation of optical transmittance is caused by the reduction of light scattering on the surface of $\text{SnO}_2:\text{Eu}^{3+}$ films, which should be related to the variable morphology of the homogeneously distributed $\text{SnO}_2:\text{Eu}^{3+}$ grains. Thus, the top-view scanning electron microscopy (SEM) images of SnO_2 and $\text{SnO}_2:\text{Eu}^{3+}$ films were measured and are shown in Figure S1, Supporting Information. The images show that the SnO_2 film appears to be flat, uniform and pinhole-free. After the introduction of Eu^{3+}

ions, many nanoparticles appear on the grain surface. Figure S2, Supporting Information shows atomic force microscopy images of SnO_2 and $\text{SnO}_2:\text{Eu}^{3+}$ films deposited on FTO substrates. The calculated data reveal that the root-mean-square roughness decreases from 29.9 to 22.1 nm with Eu^{3+} doping. Note that the smoother surface is beneficial to film-forming of the perovskite layer.^[23]

FTIR spectra is used to study the interaction between the dopant Eu^{3+} and matrix SnO_2 . As shown in Figure 1b, the peaks around 760 cm^{-1} belong to the O–Sn–O symmetric stretch, and the peaks at 895 cm^{-1} are attributed to the O–O stretching about vibration of the oxygen adsorbed on the surface of SnO_2 films. All the weaker peaks at ≈ 2180 , ≈ 2027 , and $\approx 1977\text{ cm}^{-1}$ are due to Sn–O stretching vibrations.^[23,27] All of these absorption peaks are unaffected by Eu^{3+} doping; however, for the $\text{SnO}_2:20\%\text{ Eu}^{3+}$ sample, the characteristic asymmetric stretching peaks on the SnO_2 surface shift to 486, 446, and 434 cm^{-1} ,^[27] which demonstrates that Eu^{3+} ions might enter into the SnO_2 crystal lattice and affect the SnO_2 surface.

To further clarify the interaction between Eu^{3+} and SnO_2 , the XPS spectra for SnO_2 and $\text{SnO}_2:20\%\text{ Eu}^{3+}$ films are measured and shown in Figure 1c. Clearly, the two Sn peaks and O peak are centered at ≈ 484 , ≈ 493 , and $\approx 529\text{ eV}$, respectively. Meanwhile, high-resolution Sn 3d, O 1s, and Eu 3d spectra are displayed in Figure 1d. In comparison with pristine SnO_2 films, the shifts of ≈ 0.2 and 0.05 eV of the Sn 3d and O 1s peaks, respectively, can be observed in the $\text{SnO}_2:20\%\text{ Eu}^{3+}$ films, indicating that the Eu^{3+} dopant affects the SnO_2 surface. Furthermore, the presence of trivalent Eu^{3+} can be confirmed by the observed binding energies at ≈ 1167.2 and 1139.8 eV , which are attributed to the $3d_{3/2}$ and $3d_{5/2}$ orbitals of Eu^{3+} .

The electrical properties of semi-conductive films can be characterized by the Hall Effect measurements, such as conductivity type, resistivity, mobility and carrier concentration. The average Hall coefficient, resistivity, mobility, and carrier concentration of SnO_2 and $\text{SnO}_2:20\%\text{ Eu}^{3+}$ were measured and shown in Table S1, Supporting Information, respectively. The average Hall coefficients indicate that SnO_2 and $\text{SnO}_2:20\%\text{ Eu}^{3+}$ are both well ETL films. Meanwhile the recorded resistivities, mobilities, and carrier concentrations prove Eu^{3+} doping can reduce resistivity and promote mobility in SnO_2 films. It is known that the electron mobility of ETLs is the key factor for the performance improvement of PSCs. The various ETLs are also measured by the space charge-limited current method,^[23] and the results shown in Figure 2a. It is found that the electron mobility of $\text{SnO}_2:20\%\text{ Eu}^{3+}$ is $1.48 \times 10^{-5}\text{ cm}^2\text{ V}^{-1}\text{ s}^{-1}$, which is about eight larger than that of SnO_2 ($1.97 \times 10^{-6}\text{ cm}^2\text{ V}^{-1}\text{ s}^{-1}$). High electron mobility can effectively promote electron transfer in an ETL, thus the charge consumption at the interface between the ETL and perovskite is reduced, finally resulting in improved efficiency of PSCs.

The PL spectra of the perovskite deposited on different ETL substrates are presented in Figure 2b. Compared with the FTO/ SnO_2 /perovskite sample, significant PL quenching is observed with increasing Eu^{3+} concentration in the samples on $\text{SnO}_2:\text{Eu}^{3+}$ ETL substrates. The data demonstrate optimized $\text{SnO}_2:20\%\text{ Eu}^{3+}$ presents the most appealing merits with the highest electron mobility. Figure 2c displays the normalized TRPL for perovskites on various ETLs. The lifetimes and corresponding proportions are listed in Table S2, Supporting

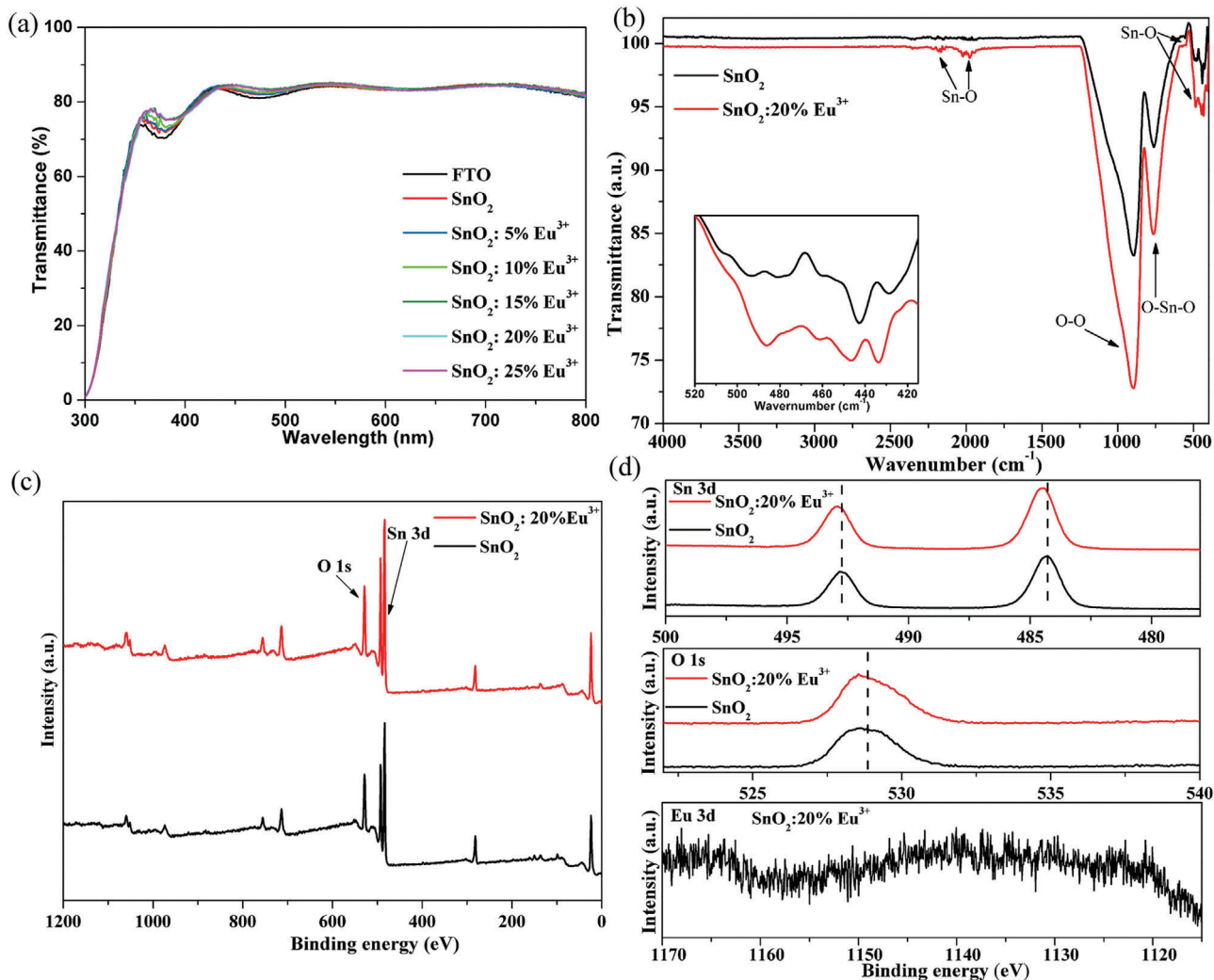


Figure 1. a) Optical transmission spectra of FTO substrates, SnO₂ and SnO₂:Eu³⁺ films on FTO substrates. b) Fourier-transform infrared spectroscopy (FTIR) spectra of SnO₂ and SnO₂:20% Eu³⁺ films. c) Typical X-ray photoelectron spectroscopy (XPS) spectra of SnO₂ and SnO₂:20% Eu³⁺ films. d) High-resolution XPS spectra of Sn 3d, O 1s, and Eu 3d of SnO₂ and SnO₂:Eu³⁺ films.

Information. The lifetime decay curves have two parts: a slow decay component τ_1 and a fast decay component τ_2 . Generally, τ_1 is attributed to the radiative recombination of free carriers captured by the traps in bulk materials and τ_2 originates from the quenching of charge carriers in the transportation process through the interfaces.^[23,28] The FTO/SnO₂/perovskite sample presents a long τ_2 lifetime of 37.55 ns, but it quickly decreases with increasing Eu³⁺ in SnO₂ films. Smaller τ_2 dominating PL decay indicates that electrons can be effectively extracted from the perovskite layer to the ETL with minimal recombination loss at the interface. In the sample of perovskite deposited on SnO₂:20% Eu³⁺, τ_1 was increased slightly to 7.65 ns, but τ_2 was considerably shortened to 3.53 ns; moreover, the lifetime contributions of τ_1 and τ_2 are 13.05% and 86.95%, respectively. These results indicate that the Eu³⁺ dopant in SnO₂:20% Eu³⁺ film leads to suppressed charge carrier recombination at the interfaces, which remarkably dominates the overall charge carrier transport process. Moreover, sharply decreased τ_2 indicates that the carrier

transfer efficiency at the interfaces can be significantly promoted by doping Eu³⁺ into SnO₂. To summarize, the reduced loss of charge carriers at the interfaces drastically improves the carrier transfer efficiency in SnO₂:20% Eu³⁺, which can be considered as a potential electron extraction layer for planar-type PSCs.

The doped europium ions in MAPbI₃ perovskite films can simultaneously reduce Pb⁰ and I⁰ defects for achieving high PCE, and they more easily concentrate at surfaces and grain boundaries or intercalate into two adjacent lattices.^[10] In our research, X-ray diffraction (XRD) patterns of MAPbI₃ on various ETL substrates (SnO₂ and SnO₂:Eu³⁺) in Figure 3a,b indicate that europium ions can spread from SnO₂:Eu³⁺ films into MAPbI₃ perovskite films. When the europium ion concentration in SnO₂ films is adjusted from 5 to 20 mol%, an obvious shift of the MAPbI₃ (110) diffraction peak is observed. Because the radii of Eu³⁺ and Pb²⁺ are 94.7 and 119 pm, respectively, the shifts of the diffraction peak indicate that Eu³⁺ may prefer to intercalate into two adjacent lattices than to enter into the perovskite crystal

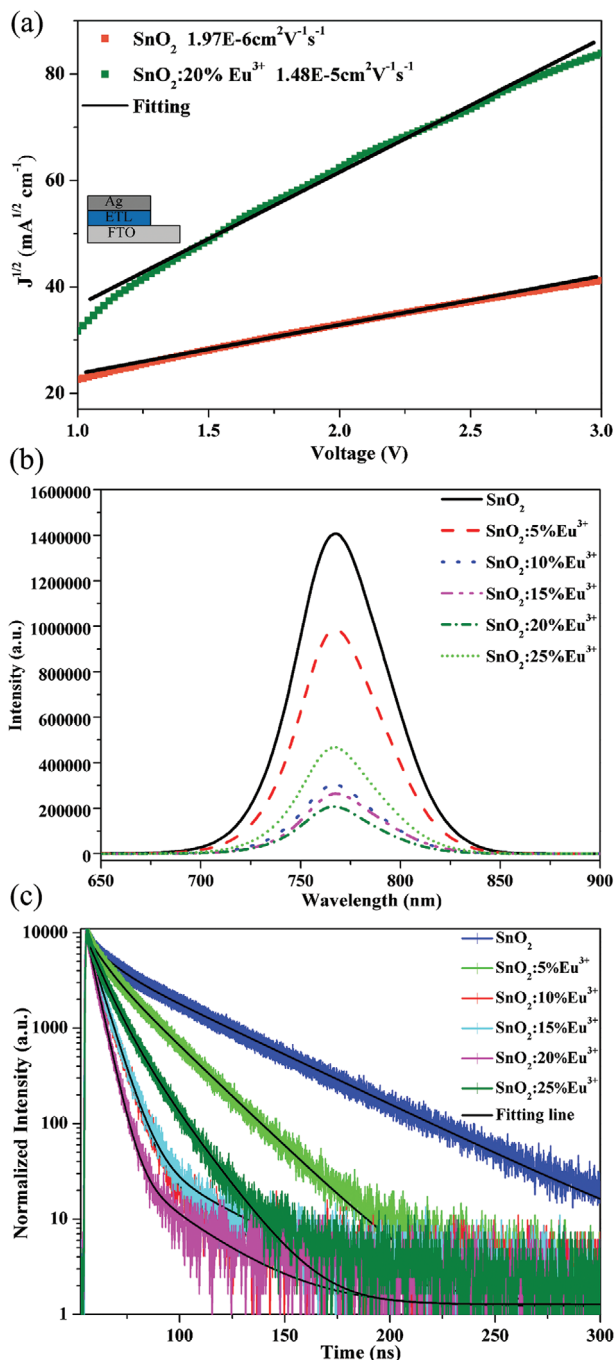


Figure 2. a) Electron mobility for SnO₂ and SnO₂:20% Eu³⁺ films; the inset shows the device structure of FTO/ETL/Ag. b) Steady-state photoluminescence (PL) and c) time-resolved photoluminescence (TRPL) spectra of perovskite films deposited on different ETL substrates.

lattice, in accordance with the reported density functional theory result.^[10] When the doping concentration of Eu³⁺ exceeds 20%, excess Eu³⁺ might enter Pb²⁺ sites of the perovskite crystal lattice. Therefore, the shift of diffraction peak would reverse, and the corresponding photovoltaic properties of PSCs would be affected.

The SIMS curves shown in Figure 3c,d present the distribution of Pb, I, Sn, and Eu along the depth direction of perovskite/SnO₂

and perovskite/SnO₂:20% Eu³⁺ films, respectively, and their spatial distribution images are presented in Figure 3e. In the crossing regions of the SIMS profiles, sharply varying Pb, I, and Sn contents means those regions are the interfaces between the perovskite and SnO₂ (or SnO₂:Eu³⁺) films. It is observed that Eu³⁺ ions are evenly distributed in the SnO₂ film, but they tend to aggregate at the interface between the perovskite and SnO₂:20% Eu³⁺ films, and subsequently, through the process of diffusion, a few Eu³⁺ ions enter the perovskite film. Therefore, the shifts of the asymmetric stretching Sn–O peaks in the FTIR spectra (Figure 1b) and the dramatically increased proportions of τ_2 lifetime in the TRPL spectra (Figure 2c) are observed, which are both related to the aggregation of Eu³⁺ at the interface between the perovskite and SnO₂:Eu³⁺ films. An EDS mapping image of perovskite/SnO₂:Eu³⁺ film is presented in Figure 3f. Although the amount of Eu³⁺ ions pervading the perovskite film is very low, their distribution is uniform throughout the perovskite film.

The surface coverage of perovskite films is also very important for high-performance PSCs.^[27–29] The aggregation of Eu³⁺ on the top interface of SnO₂:Eu³⁺ films may affect the nucleation and growth of perovskite films. A smaller contact angle can result in a reduced Gibbs free energy facilitating heterogeneous nucleation; meanwhile, the formation of more crystal nuclei will accelerate the process of thin film growth from nuclei to island structures, then to networked, and finally into a continuous film.^[23,30,31] The contact angles of SnO₂ and SnO₂:Eu³⁺ films are measured and presented in Figure S3, Supporting Information. All calculated contact angles indicate that increased concentration of dopant Eu³⁺ in SnO₂:Eu³⁺ films reduces the contact angle on the surface, and moreover, the contact angle is a minimum of 10.2° on the surface of SnO₂:20% Eu³⁺ films, which can result in lower surface energy and accelerated perovskite crystallization during the growth of the networked structure.^[30,32] However, the grain sizes of perovskite films are not obviously affected by the different substrates, as shown in the SEMs of Figure S4, Supporting Information.

Grain boundary plays a critical role in determining the charge collection efficiency and stability of PSCs. The passivation of grain boundary can reduce the trap densities of perovskite films to improve the performance of PSCs. Different grain boundary passivation methods are being studied, such as introducing the PbI₂-rich phase at grain boundaries in MAPbI₃ PSCs,^[33] or using carbon quantum dots additive to passivate the uncoordinated lead ions on grain boundaries of MAPbI₃ PSCs.^[34] In our work, the aggregated Eu³⁺ at the grain boundaries and the interfaces can reduce Pb⁰ and I⁰ defects further to passivate grain boundaries. Thus the trap densities of perovskites on different ETLs are evaluated by the space charge-limited current measurements of electron-only devices fabricated with the structure ITO (indium tin oxide)/ETL/perovskite/PCBM (phenyl-C61-butyric acid methyl ester)/Ag, and the corresponding dark current–voltage (*I*–*V*) curves are shown in Figure S5, Supporting Information. At low bias voltage, the linear correlation shown as red lines indicates an ohmic response. When the bias voltage increases above the kink point, the current suddenly increases with a non-linear correlation (cyan line), which reveals that the traps in the perovskite film are totally filled. The bias voltage corresponding to the kink point between the linear and nonlinear correlation is defined as the trap-filled limit voltage (V_{TFL}). The trap densities

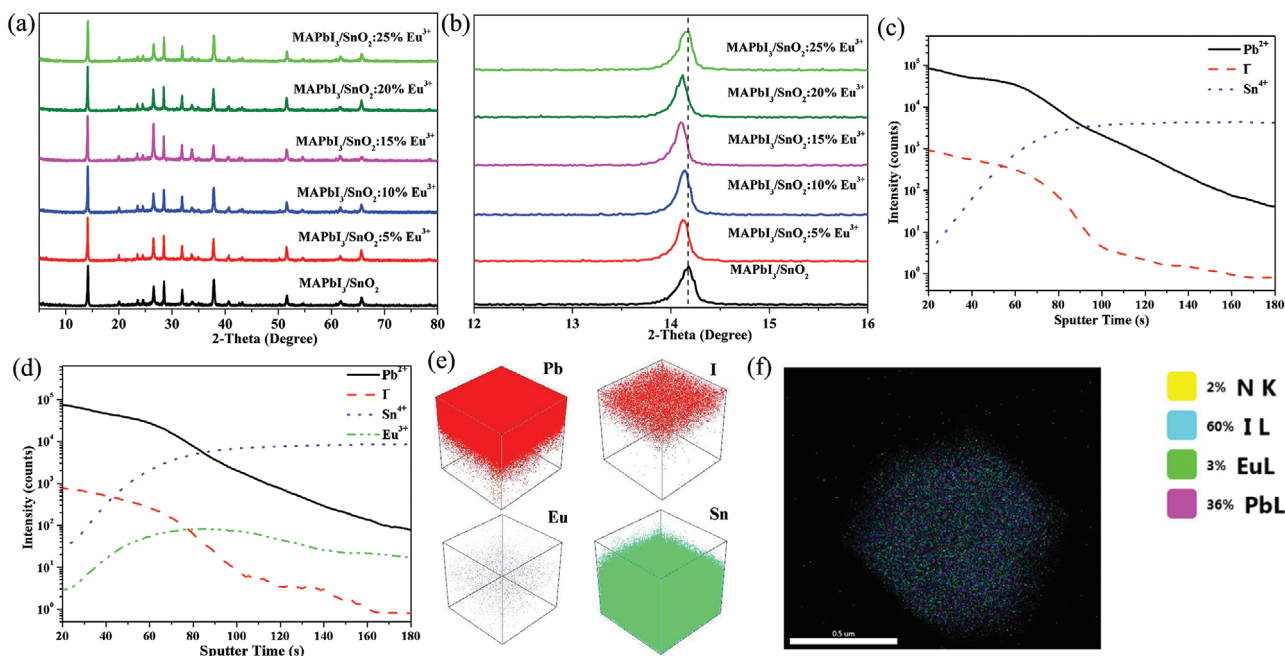


Figure 3. a) XRD patterns and b) enlarged XRD patterns of MAPbI₃ on SnO₂ and SnO₂:Eu³⁺ ETL substrates. Secondary ion mass spectroscopy (SIMS) of c) perovskite/SnO₂ and d) perovskite/SnO₂:20% Eu³⁺ films. e) The spatial distribution of Pb, I, Eu, and Sn in perovskite/SnO₂:Eu³⁺ films. f) Energy dispersive spectroscopy (EDS) mapping image of perovskite/SnO₂:Eu³⁺ film.

(N_t) of the perovskites on different ETLs are calculated by the equation $N_t = (2V_{\text{TFL}}\epsilon\epsilon_0)/(eL^2)$,^[35,36] where ϵ and ϵ_0 are the relative dielectric constant for MAPbI₃ perovskite and vacuum permittivity, respectively, e is the electron charge and L is the thickness of the MAPbI₃ perovskite film. It is obvious that the trap densities of the perovskites were reduced from 1.69×10^{16} to $1.31 \times 10^{16} \text{ cm}^{-3}$ by increasing the amount of Eu³⁺ dopant to 20% in the SnO₂ substrate, and this reduction is attributed to the passivation of grain boundaries caused by increased Eu³⁺ at grain boundaries and interfaces.

According to the above discussion, SnO₂:Eu³⁺ is expected to be a better ETL for PSCs than the pristine SnO₂ film. Therefore, planar-type PSCs with different SnO₂ films as ETL substrates are designed with the structure shown in Figure 4a. MAPbI₃ and Spiro-OMeTAD are used as the photon absorber layer and hole-transport layer, respectively. The thicknesses of the perovskites are nearly unchanged by doping 20% Eu³⁺ into SnO₂ film, as shown in the cross-sectional SEM images of PSCs in Figure S6, Supporting Information.

Figure 4b and Figure S7, Supporting Information present the J - V curves of PSCs on various ETL substrates, and the corresponding key parameters, such as the open-circuit voltage (V_{oc}), the short-circuit current (J_{sc}), fill factor (FF), and PCE are all summarized in Table S3, Supporting Information. The maximum PCE of the devices based on the SnO₂ ETL substrate is 18.66%, with the corresponding $V_{\text{oc}} = 1.06 \text{ V}$, $J_{\text{sc}} = 22.57 \text{ mA cm}^{-2}$, and $\text{FF} = 77.77\%$. It is exciting that the optimal PCE can be increased to 20.14% by changing the SnO₂ ETL to SnO₂:20% Eu³⁺ ETL, with corresponding V_{oc} and FF dramatically increased to 1.13 V and 78.76%, respectively. The increased FF are due to the reduced trap density in perovskite film; however, the improved V_{oc} should be attributed to the reduced energy loss in MAPbI₃ PSCs.^[37]

Mott-Schottky analysis based on capacitance-voltage (C - V) measurement can be used to investigate the change of built-in electric field and is carried out to further understand the charge carrier trapping and accumulating behaviors with the incorporation of Eu³⁺ dopant.^[38-41] Figure 4c presents the C^{-2} - V plots for MAPbI₃ perovskite PSCs, and the corresponding values of the built-in electric fields (V_{bi}) in the PSCs based on different ETLs are obtained from the Mott-Schottky equation $C^{-2} = (2(V_{\text{bi}} - V))/(A^2\epsilon\epsilon_0N)$, where C is the capacitance under applied voltage, V_{bi} is the built-in potential, V is the applied bias, A is the device area, ϵ is the relative permittivity, ϵ_0 is the vacuum permittivity, and N is the free carrier concentration at the edge of the depletion layer.^[42,43] The V_{bi} for the PSC coated on SnO₂:20% Eu³⁺ ETL is 0.972 V, which is larger than 0.942 V of the control device without europium dopant. The enhanced built-in potential provides more driving force to separate the photogenerated charge carriers, resulting in an extended depletion region, which suppresses electron-hole recombination, finally contributing to the increase of V_{oc} .

On the other hand, the V_{oc} is also determined by the quasi-Fermi level separation of electrons and holes in the light-dependent dynamic equilibrium condition, and the reduced charge carrier recombination and fewer traps within the bandgap can narrow the distribution of defect states and elevate the quasi-Fermi levels of electrons.^[44] As shown in Figure S5, Supporting Information, the reduced trap density from 1.69×10^{16} to $1.31 \times 10^{16} \text{ cm}^{-3}$ can be obtained by coating MAPbI₃ perovskite film on SnO₂:20% Eu³⁺ substrate. The significantly reduced trap-assisted recombination elevates the quasi-Fermi level of electrons, and thus greater quasi-Fermi level separation can be obtained. As a result, the PSCs fabricated on the SnO₂:20%Eu³⁺ substrate exhibit a higher V_{oc} compared to the control PSCs on the SnO₂ substrate.

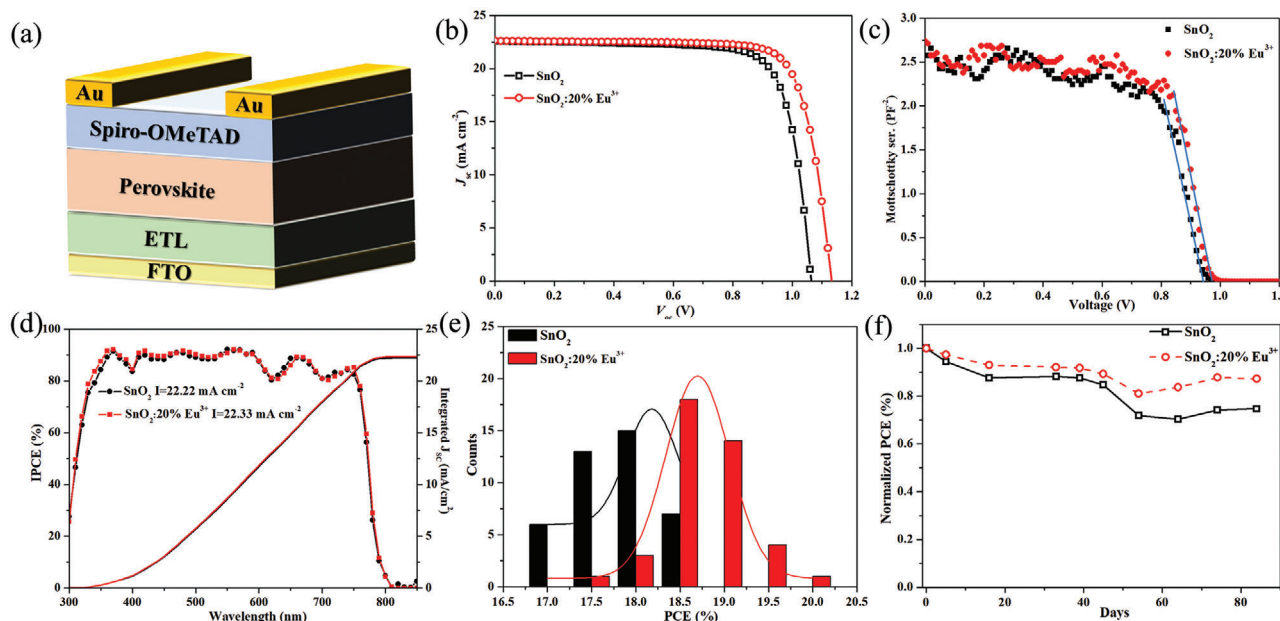


Figure 4. a) The designed device configuration. b) Current density–voltage (J - V) curves, c) Mott–Schottky plots and d) The incident-photon-to-charge conversion efficiency (IPCE) of the PSCs with different ETL substrates. The integrated current densities from the IPCE curves were recorded under the AM1.5G spectrum. e) The PCE distribution of the PSCs based on the different ETLs. f) Long-term stability test for planar-type PSC devices with different ETLs without any encapsulation under ambient conditions (35% humidity in the dark).

Electrical impedance spectroscopy is carried out to monitor the transfer resistance in PSCs. The Nyquist plots of the PSCs fabricated on different SnO₂ or SnO₂:Eu³⁺ films recorded at V_{oc} under dark conditions are shown in Figure S8, Supporting Information, and the corresponding equivalent circuit is shown in Figure S9, Supporting Information. It is known that the recombination resistance (R_{rec}) is in the low-frequency range,^[42] and, in our fabricated PSCs, it increases with increased Eu³⁺ doping in the SnO₂ films. Compared to the control PSCs, the device fabricated on SnO₂:20% Eu³⁺ substrate shows the largest R_{rec} of 289 Ω , which can effectively inhibit charge recombination at grain boundaries and the interface, because the aggregated Eu³⁺ at grain boundaries and the interface decrease the amount of negative defects Pb⁰ and I⁰.

Figure 4d shows the IPCE spectra and the integrated J_{sc} values versus wavelength for the PSCs based on different ETLs. The effect on IPCE of Eu³⁺ doping in the ETL is divided into two parts: 1) In the UV region of 300–370 nm, the IPCE intensity is enhanced by Eu³⁺ doping due to the f - f transitions absorption of Eu³⁺.^[45–49] The absorption of Eu³⁺ reduces the damage to the perovskite film from UV light, resulting in the obvious increase of the IPCE; 2) The enhancement of IPCE in the region of 370–550 nm is attributed to the increased transmittance of ITO/SnO₂:20% Eu³⁺ substrate. The highest observed IPCE value reaches 92%. Meanwhile, the integrated J_{sc} increases from 22.22 to 22.33 mA cm⁻² by using SnO₂:20% Eu³⁺ film as the ETL substrate, which indicates SnO₂:20% Eu³⁺ is an excellent ETL for application in PSCs. The stabilized power output of the device with SnO₂:20% Eu³⁺ ETL is shown in Figure S10, Supporting Information. While maintaining an external bias near the maximum power output point (0.88 V), the stabilized photocurrent for the

PSC with SnO₂:20% Eu³⁺ ETL is 21.37 mA cm⁻². The results indicate that SnO₂:20% Eu³⁺ ETL is beneficial to the illumination stability of the MAPbI₃ perovskite device.

Stability and repeatability are also very important characteristics for PSCs. The PCE distribution histograms for devices with different ETLs are presented in Figure 4e. The device based on SnO₂:20% Eu³⁺ substrate exhibits excellent repeatability in contrast to that based on the pristine SnO₂ substrate. Figure 4f shows normalized PCE of the different device exposed to an ambient atmosphere (\approx 35% humidity) during 84 days in the dark. It is clear that the device based on SnO₂:20% Eu³⁺ substrate maintains 87% of its initial PCE on the 84th day, but the device coated on SnO₂ substrate has decreased to 75% of its initial PCE under the same storage conditions. Their stabilities at higher temperature in N₂ atmosphere, even under continuous illumination and higher humidity are both investigated and shown in Figure S11a,b, Supporting Information, respectively. After storing devices in dark with N₂ atmosphere at 80 $^{\circ}$ C for 500 min, the PCE of control device has dropped to 30% of its initial value. But the decrease can be retarded to be very slow by 20% Eu³⁺ doped in SnO₂, thus the device coated on SnO₂:20% Eu³⁺ substrate just decreases to 65% of its initial PCE under the same storage conditions. Even under continuous 100 mW cm⁻² illumination and 40–50% humidity at 60 $^{\circ}$ C for 300 min, the SnO₂:20% Eu/Perovskite device can still keep 50% of its initial PCE, but the PCE of SnO₂/Perovskite device has drop to 40% of its initial value. The comparison demonstrates that the PSCs coated on SnO₂:20% Eu³⁺ show more excellent stability, which is due to the europium ions can effectively passivate the defects at the grain boundaries and interfaces preventing moisture permeation, further resulting in the improved environmental stability.^[50]

3. Conclusion

This work describes a novel dual-functional method to simultaneously optimize charge transport characteristics of the perovskite and ETL layers which account for the enhancement of performance of the corresponding PSCs. An effective $\text{SnO}_2\cdot\text{Eu}^{3+}$ ETL is developed, and the champion device incorporating it achieves a PCE of 20.14%, showing excellent stability by maintaining 87% of its initial efficiency after storage in ambient atmosphere for 84 days. The excellent performance of the PSCs is attributed to the dual-passivation effect of europium ions in SnO_2 . The uniformly distributed europium dopants reduce the trap defects in the SnO_2 film, resulting in increased electron mobility of the ETL. The aggregation of europium ions at the interface between the perovskite and SnO_2 films is beneficial for improving electron transport through the interface by reducing the charge accumulation at the interface. Moreover, the aggregated europium ions passivate the perovskite by reducing the trap density in the grain boundaries, which is favorable to the V_{oc} and FF of PSCs. Meanwhile, the aggregated europium ions both on the grain boundaries and interface suppress perovskite degradation by preventing moisture permeation. Our dual-functional method provides a promising direction toward simultaneously optimizing the ETL and perovskite films, and we believe that the present work will facilitate the development of perovskite photovoltaics.

4. Experimental Section

Materials: $\text{SnCl}_2\cdot 2\text{H}_2\text{O}$ (98%) was purchased from Macklin. Thioglycolic acid was purchased from Sigma-Aldrich. $\text{EuCl}_3\cdot 6\text{H}_2\text{O}$ (99.99%) was purchased from CIVI-CHEM. PbI_2 (99.9985%) was purchased from Alfa Aesar. MAI (99.5%) was purchased from Xi'an Polymer Light Technology Corp. Urea, 4-tert-butylpyridine (TBP) and bis(trifluoromethane) sulfonamide lithium salt (Li-TFSI) were purchased from Aladdin. HCl (37 wt%) and chlorobenzene ($\geq 99.0\%$) were purchased from Sinopharm Chemical Reagent Corporation Co., Ltd. Spiro-OMeTAD ($\geq 99.0\%$) was ordered from Youxuan Tech. 4-Hydroxybutanoic acid lactone (GBL) and dimethyl sulfoxide (DMSO) were ordered from Alfa-Aesar.

Device Fabrication: The FTO-coated glass (2.5×2.5 cm) was cleaned by sequential sonication in acetone, isopropanol, and ethanol for 30 min each time and then dried under air flow and treated by ozone plasma for 6 min. The undoped and Eu-doped SnO_2 layers were prepared by the chemical bath deposition method. Briefly, for the preparation of undoped SnO_2 ETL, 0.5 g of urea was dissolved in 40 mL deionized water, and then 10 mL thioglycolic acid and 500 mL HCl were added to the aqueous solution. Finally, $\text{SnCl}_2\cdot 2\text{H}_2\text{O}$ was dissolved in the solution at 0.002 M concentration followed by stirring for 2 min. The clean FTO substrates were immersed in the aqueous solution at 70 °C for 3 h, followed by rinsing in a deionized water sonication bath for 2 min. Then they were dried with flowing air and heat-treated for 1 h at 180 °C in air. For the preparation of (5, 10, 15, 20, and 25 mol%) Eu-doped SnO_2 ETLs, $\text{EuCl}_3\cdot 6\text{H}_2\text{O}$ was added directly to the prepared aqueous solution before immersing the cleaned FTO substrates.

The MAPbI_3 perovskite solution (1.4 M) was comprised of MAI and PbI_2 in 1 mL of GBL/DMSO = 7:3 (v/v). The solution was stirred at room temperature for 12 h. Then the FTO/ETL substrates were treated by ozone plasma for 6 min. The solution was spin-coated onto the FTO/ETL substrate by a consecutive two-step process at 1000 rpm for 10 s and followed by 3000 rpm for 40 s. During the second step, 200 mL of chlorobenzene was dropped onto the substrate. The films were then annealed at 100 °C for 10 min in a nitrogen-filled glovebox. 90 mg mL⁻¹ spiro-OMeTAD in 1 mL chlorobenzene with the addition of 36 mL TBP and 22 mL Li-TFSI solution (520 mg in 1 mL acetonitrile) was spin-coated onto the perovskite films at 5000 rpm for 40 s. The samples were kept in a desiccator overnight.

Finally, 80 nm gold electrodes were deposited on the top of each cell by a thermal evaporator.

Device Characterization: XRD spectra were obtained using a D/MAX 2400 diffractometer with Cu K α radiation (Rigaku). Transmittance spectra were acquired on a PerkinElmer UV-Lambda 950 instrument. PL (excitation at 510 nm, front-side excitation) and TRPL spectra (excitation at 510 nm and emission at 768 nm, front-side excitation) were measured with a PicoQuant FT-300. Water contact angles were measured using a Data-Physics OCA 20. The surface morphologies of the perovskite films and the SnO_2 films were characterized by SEM (FE-SEM; SU-8020, Hitachi) at an acceleration voltage of 5 kV. XPS measurements were carried out by using a photoelectron spectrometer (ESCALAB 250Xi, Thermo Fisher Scientific). SIMS curves were recorded by the time of flight secondary ion mass spectrometry (TOF SIMS IV, ION TOF GmbH). The J - V performance of the perovskite solar cells was analyzed using a Keithley 2400 Source Meter under ambient conditions at room temperature, and the illumination intensity was 100 mW cm⁻² (AM 1.5G Oriel solar simulator) with scan rate 0.2 V s⁻¹. The device area of 0.09 cm² was defined by a metal aperture to avoid light scattering from the metal electrode into the device during the measurement. The IPCE was characterized on a QTest Station 2000ADI system (Crowntech Inc., USA), and the light source was a 300 W xenon lamp. The monochromatic light intensity for the IPCE measurement was calibrated with a reference silicon photodiode. The Hall Effect measurements were recorded by the Hall Effect Measurement System (HMS-3000).

Supporting Information

Supporting Information is available from the Wiley Online Library or from the author.

Acknowledgements

This research was supported by the National Key Research Program of China (2016YFA0202403), the National Natural Science Foundation of China (21603140) and the 111 Project (B14041).

Conflict of Interest

The authors declare no conflict of interest.

Keywords

europium, perovskite, photovoltaics, solar cells

Received: April 21, 2020
Revised: October 30, 2020
Published online: January 29, 2021

- [1] A. Kojima, K. Teshima, Y. Shirai, T. Miyasaka, *J. Am. Chem. Soc.* **2009**, *131*, 6050.
- [2] M. M. Lee, J. Teuscher, T. Miyasaka, T. N. Murakami, H. J. Snaith, *Science* **2012**, *338*, 643.
- [3] H. Zhou, Q. Chen, G. Li, S. Luo, T. Song, H. S. Duan, Z. Hong, J. You, Y. Liu, Y. Yang, *Science* **2014**, *345*, 542.
- [4] J. H. Im, I. H. Jang, N. Pellet, M. Grätzel, N. G. Park, *Nat. Nanotechnol.* **2014**, *9*, 927.
- [5] M. Yang, Y. Zhou, Y. Zeng, C. S. Jiang, N. P. Padture, K. Zhu, *Adv. Mater.* **2015**, *27*, 6363.
- [6] O. Malinkiewicz, A. Yella, Y. H. Lee, G. M. Espallargas, M. Graetzel, M. K. Nazeeruddin, H. J. Bolink, *Nat. Photonics* **2014**, *8*, 128.

- [7] W. S. Yang, J. H. Noh, N. J. Jeon, Y. C. Kim, S. Ryu, J. Seo, S. Il Seok, *Science* **2015**, *348*, 1234.
- [8] W. S. Yang, B. W. Park, E. H. Jung, N. J. Jeon, Y. C. Kim, D. U. Lee, S. S. Shin, J. Seo, E. K. Kim, J. H. Noh, S. Il Seok, *Science* **2017**, *356*, 1376.
- [9] National Renewable Energy Laboratory (NREL) Efficiency chart **2018**; www.nrel.gov/pv/assets/pdfs/pv-efficiency-chart.20181214.pdf. Accessed January 2021.
- [10] L. Wang, H. Zhou, J. Hu, B. Huang, M. Sun, B. Dong, G. Zheng, Y. Huang, Y. Chen, L. Li, Z. Xu, N. Li, Z. Liu, Q. Chen, L. Sun, C. Yan, *Science* **2019**, *363*, 265.
- [11] N. H. Tiep, Z. Ku, H. J. Fan, *Adv. Energy Mater.* **2016**, *6*, 1501420.
- [12] Y. Rong, L. Liu, A. Mei, X. Li, H. Han, *Adv. Energy Mater.* **2015**, *5*, 1501066.
- [13] T. A. Berhe, W. N. Su, C. H. Chen, C. J. Pan, J. H. Cheng, H. M. Chen, M. C. Tsai, L. Y. Chen, A. A. Dubaleb, B. J. Hwang, *Energy Environ. Sci.* **2016**, *9*, 323.
- [14] J. M. Frost, K. T. Butler, F. Brivio, C. H. Hendon, M. Schilfgaarde, A. Walsh, *Nano Lett.* **2014**, *14*, 2584.
- [15] Z. Yu, L. Sun, *Adv. Energy Mater.* **2015**, *5*, 1500213.
- [16] W. Li, J. Li, G. Niu, L. Wang, *J. Mater. Chem. A* **2016**, *4*, 11688.
- [17] W. Li, W. Zhang, S. V. Reenen, R. J. Sutton, J. Fan, A. A. Haghighirad, M. B. Johnston, L. Wang, H. J. Snaith, *Energy Environ. Sci.* **2016**, *9*, 490.
- [18] T. Niu, J. Lu, R. Munir, J. Li, D. Barrit, X. Zhang, H. Hu, Z. Yang, A. Amassian, K. Zhao, S. F. Liu, *Adv. Mater.* **2018**, *30*, 1706576.
- [19] T. Niu, J. Lu, M. C. Tang, D. Barrit, D. M. Smilgies, Z. Yang, J. Li, Y. Fan, T. Luo, I. McCulloch, A. Amassian, S. F. Liu, K. Zhao, *Energy Environ. Sci.* **2018**, *11*, 3358.
- [20] H. Chen, Q. Luo, T. Liu, J. Ren, S. Li, M. Tai, H. Lin, H. He, J. Wang, N. Wang, *Small* **2019**, *15*, 1904372.
- [21] W. Zhou, D. Li, Z. Xiao, Z. Wen, M. Zhang, W. Hu, X. Wu, M. Wang, W. H. Zhang, Y. Lu, S. Yang, S. Yang, *Adv. Funct. Mater.* **2019**, *29*, 1901026.
- [22] W. Chen, Y. Wang, G. Pang, C. W. Koh, A. B. Djurišić, Y. Wu, B. Tu, F. Liu, R. Chen, H. Y. Woo, X. Guo, Z. He, *Adv. Funct. Mater.* **2019**, *29*, 1808855.
- [23] D. Yang, R. Yang, K. Wang, C. Wu, X. Zhu, J. Feng, X. Ren, G. Fang, S. Priya, S. F. Liu, *Nat. Commun.* **2018**, *9*, 3239.
- [24] Q. An, P. Fassl, Y. J. Hofstetter, D. B. Koch, A. Bausch, P. E. Hopkinson, Y. Vaynzof, *Nano Energy* **2017**, *39*, 400.
- [25] B. Zhang, Z. Song, J. Jin, W. Bi, H. Li, C. Chen, Q. Dai, L. Xu, H. Song, *J. Colloid Interface Sci.* **2019**, *553*, 14.
- [26] G. Yang, H. Lei, H. Tao, X. Zheng, J. Ma, Q. Liu, W. Ke, Z. Chen, L. Xiong, P. Qin, Z. Chen, M. Qin, X. Lu, Y. Yan, G. Fang, *Small* **2017**, *13*, 1601769.
- [27] S. Zhuang, X. Xu, B. Feng, J. Hu, Y. Pang, G. Zhou, L. Tong, Y. Zhou, *ACS Appl. Mater. Interfaces* **2014**, *6*, 613.
- [28] Y. Li, L. Meng, Y. M. Yang, G. Xu, Z. Hong, Q. Chen, J. You, G. Li, Y. Yang, Y. Li, *Nat. Commun.* **2016**, *7*, 10214.
- [29] A. A. Zhumekenov, V. M. Burlakov, M. I. Saidaminov, A. Alofi, M. A. Haque, B. Turedi, B. Davaasuren, I. Dursun, N. Cho, A. M. El-Zohry, M. D. Bastiani, A. Giugni, B. Torre, E. D. Fabrizio, O. F. Mohammed, A. Rothenberger, T. Wu, A. Goriely, O. M. Bakr, *ACS Energy Lett.* **2017**, *2*, 1782.
- [30] H. Zhao, S. Wang, M. Sun, F. Zhang, X. Li, Y. Xiao, *J. Mater. Chem. A* **2018**, *6*, 10825.
- [31] T. Salim, S. Sun, Y. Abe, A. Krishna, A. C. Grimdale, Y. M. Lam, *J. Mater. Chem. A* **2015**, *3*, 8943.
- [32] P. Fu, L. Huang, W. Yu, D. Yang, G. Liu, L. Zhou, J. Zhang, C. Li, *Nano Energy* **2015**, *13*, 275.
- [33] M. N. F. Hoque, R. He, J. Warzywoda, Z. Fan, *ACS Appl. Mater. Interfaces* **2018**, *10*, 30322.
- [34] Y. Ma, H. Zhang, Y. Zhang, R. Hu, M. Jiang, R. Zhang, H. Lv, J. Tian, L. Chu, J. Zhang, Q. Xue, H. L. Yip, R. Xia, X. Li, W. Huang, *ACS Appl. Mater. Interfaces* **2019**, *11*, 3044.
- [35] D. Yang, R. Yang, X. Ren, X. Zhu, Z. Yang, C. Li, S. F. Liu, *Adv. Mater.* **2016**, *28*, 5206.
- [36] H. Jiang, Z. Yan, H. Zhao, S. Yuan, Z. Yang, J. Li, B. Liu, T. Niu, J. Feng, Q. Wang, D. Wang, H. Yang, Z. Liu, S. F. Liu, *ACS Appl. Energy Mater.* **2018**, *1*, 900.
- [37] S. Yang, H. Zhao, Y. Han, C. Duan, Z. Liu, S. F. Liu, *Small* **2019**, *15*, 1904387.
- [38] P. N. Murgatroyd, *J. Phys. D: Appl. Phys.* **1970**, *3*, 151.
- [39] R. H. Bube, *J. Appl. Phys.* **1962**, *33*, 1733.
- [40] J. M. Luther, M. Law, M. C. Beard, Q. Song, M. O. Reese, R. J. Ellingson, A. J. Nozik, *Nano Lett.* **2008**, *8*, 3488.
- [41] Z. Jin, A. Wang, Q. Zhou, Y. Wang, J. Wang, *Sci. Rep.* **2016**, *6*, 37106.
- [42] D. Bai, J. Zhang, Z. Jin, H. Bian, K. Wang, H. Wang, L. Liang, Q. Wang, S. F. Liu, *ACS Energy Lett.* **2018**, *3*, 970.
- [43] D. Yang, R. Yang, J. Zhang, Z. Yang, S. F. Liu, C. Li, *Energy Environ. Sci.* **2015**, *8*, 3208.
- [44] K. Wang, L. Zheng, T. Zhua, X. Yao, C. Yi, X. Zhang, Y. Cao, L. Liu, W. Hu, X. Gong, *Nano Energy* **2019**, *61*, 352.
- [45] J. Gou, J. Fan, S. Zuo, M. Lou, Y. Chen, X. Zhou, Y. Yang, B. Yu, S. F. Liu, *J. Am. Chem. Soc.* **2017**, *100*, 4011.
- [46] T. Moon, S. T. Hwang, D. R. Jung, D. Son, C. Kim, J. Kim, M. Kang, B. Park, *J. Phys. Chem. C* **2007**, *111*, 4164.
- [47] J. Kong, W. Zheng, Y. Liu, R. Li, E. Ma, H. Zhu, X. Chen, *Nanoscale* **2015**, *7*, 11048.
- [48] S. D. Meetei, S. D. Singh, *J. Alloys Compd.* **2014**, *587*, 143.
- [49] X. Yu, L. Zhang, X. Xu, T. Wang, H. Yu, T. Jiang, Q. Jiao, Z. Yang, D. Zhou, J. Qiu, *J. Lumin.* **2014**, *145*, 114.
- [50] Z. Chu, M. Yang, P. Schulz, D. Wu, X. Ma, E. Seifert, L. Sun, X. Li, K. Zhu, K. Lai, *Nat. Commun.* **2017**, *8*, 2230.